# A Hybrid Finite-Element–Modal-Expansion Method With a New Type of Curvilinear Mapping for the Analysis of Microwave Passive Devices

Enrica Martini, *Member, IEEE*, Giuseppe Pelosi, *Fellow, IEEE*, and Stefano Selleri, *Senior Member, IEEE*

***Abstract*—A hybrid finite-element–modal-expansion procedure for the three-dimensional analysis of passive microwave devices exploiting higher order vector basis functions and an innovative class of curved elements is presented. If modal expansions on ports are not analytically known, they can be numerically obtained via a preliminary two-and-one-half-dimensional finite-element analysis; curved triangular and tetrahedrical elements are defined by a rational Bézier mapping, which provides a remarkable increase in accuracy and flexibility over the conventional polynomial mapping without a significant increase in computational burden. Numerical results are provided to illustrate the efficiency and feasibility of the proposed technique.**

***Index Terms*—Finite-element method (FEM), geometric modeling, microwave devices.**

## I. Introduction

THE finite-element method (FEM) is among the most versatile numerical methods for electromagnetics, thanks to its capability to operate over unstructured grids. In particular, discretizations based on triangles [two-dimensional (2-D)] and tetrahedra [three-dimensional (3-D)] are the most flexible; indeed, they can exactly fit every domain delimited by straight boundaries. Nevertheless, curved boundaries are often present in real problems; in these cases, the efficiency of the analysis can be greatly enhanced by using elements with curved sides or faces [1]. Suitable curved elements are particularly required when higher order basis functions are used since these latter allow larger elements to be used to achieve a given accuracy.

Curved elements can be generated by distorting simple forms through a nonlinear mapping of the local coordinates in the Cartesian coordinates [2]. For node-based finite elements, this mapping is usually performed via the same class of functions used as bases for unknown expansion [1] even if the degree of approximation is not necessarily the same. As far as vector finite elements are concerned, 3-D covariant projection curved elements were proposed in [3] and were subsequently used for the solution of eigenvalue problems [4], but in these papers, the issue of the choice of curvilinear mapping is not explicitly addressed. In [5], a systematic procedure for the construction of higher order and curvilinear vector finite elements was outlined; successively, various kind of such elements have been devised and applied to the analysis of resonant cavities [4] and waveguide discontinuities [6], but usually the functions used for the coordinate transformations are the conventional interpolatory polynomials. However, more general transformations are required for an exact representation of arbitrary geometries.

A different kind of mapping based on nonuniform rational B-spline (NURBS) was proposed for 2-D FEM with quadrilateral elements [7]. More recently, a new class of curved tetrahedral elements for numerical methods, based on rational Bézier volumes [8], has been presented and its effectiveness has been demonstrated by analyzing a simple cavity problem [9]. Rational coordinate transformations offer much more flexibility than polynomial ones, even though they exhibit a comparable computational cost since only polynomial functions are involved. This allows complex shapes, including those delimited by quadric surfaces, to be exactly represented by means of a small number of elements. Furthermore, the majority of the available computer-aided geometric design (CAGD) tools are based on NURBS meshes and it is quite fast and easy to obtain Bézier meshes from NURBS representations [8].

In this paper, a rational Bézier mapping is embedded in a procedure combining a 3-D FEM and modal expansions (obtained either analytically or numerically via a two–and–one–half–dimensional (2.5-D) FEM approach [10]) for the electromagnetic characterization of microwave passive devices. Similar approaches for the analysis of microwave junctions and waveguide discontinuities have been presented in several papers [11]–[13] and are also exploited by some commercial softwares; however, in these cases, zeroth- or, at best, first-order vector basis functions and rectilinear elements are used. Higher order basis functions defined over rectilinear prism elements were used in [14]. In this paper, higher order vector basis functions are combined with the innovative class of curvilinear tetrahedra presented in [9], which allows to fully exploit the basis efficiency by eliminating geometric approximation error.

The Bézier mapping and higher order vector basis functions are presented in Section II. Section III outlines the hybrid formulation. Section IV shows some numerical results to prove the effectiveness of the proposed procedure. Finally, Section V will draw some conclusions.

Manuscript received September 4, 2002; revised January 10, 2003.

E. Martini was with the Department of Electronics and Telecommunications, University of Florence, I-50134 Florence, Italy. She is now with the Department of Information Engineering, University of Siena, I-53100, Siena, Italy.

G. Pelosi and S. Selleri are with the Department of Electronics and Telecommunications, University of Florence, I-50134 Florence, Italy.

Digital Object Identifier 10.1109/TMTT.2003.812571

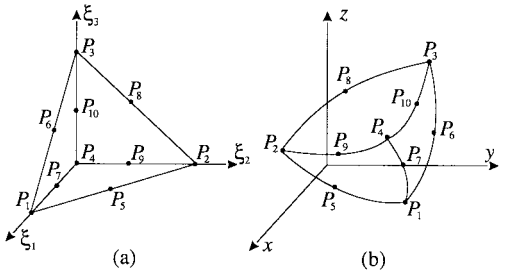


Fig. 1. Interpolatory polynomial transformation with $n = 2$. (a) Basic parent tetrahedron. (b) Curved tetrahedron. Interpolation points are shown.

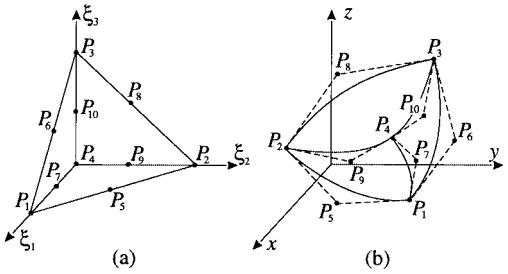


Fig. 2. Rational Bézier transformation with $n = 2$. (a) Basic parent tetrahedron. (b) Curved tetrahedron. Control points and Bézier grid are shown.

## II. Curvilinear Higher Order Elements

The position of a point $P$ inside a tetrahedron with vertices $P_1, P_2, P_3, P_4$ can be determined in terms of barycentric coordinates [8] $\boldsymbol{\xi} = (\xi_1, \xi_2, \xi_3, \xi_4)$, which are defined by

$$P = \xi_1 P_1 + \xi_2 P_2 + \xi_3 P_3 + \xi_4 P_4 \tag{1}$$

subject to the constraints

$$\xi_1, \xi_2, \xi_3, \xi_4 \geqslant 0 \quad \xi_1 + \xi_2 + \xi_3 + \xi_4 = 1. \tag{2}$$

In the following, the first three barycentric coordinates will be taken as independent and the fourth as dependent.

A curved tetrahedron is obtained through a univalent mapping of the basic parent element, defined in the local $(\xi_1, \xi_2, \xi_3)$ space [see Fig. 1(a)], into the real element in the global $(x, y, z)$ space. The simplest and most common curved elements are those belonging to the Lagrange family [2]. For a degree $n$ mapping, $N = (n+1)(n+2)(n+3)/6$ points located on a regular grid in the local space are considered and, for each of them, the global coordinates $P_m = (x_m, y_m, z_m)$ are assigned. The local coordinates of these points are $(\xi_{1_m}, \xi_{2_m}, \xi_{3_m}, \xi_{4_m}) = (i_m/n, j_m/n, k_m/n, l_m/n)$ with $i_m, j_m, k_m, l_m$ positive integers such that $i_m + j_m + k_m + l_m = n$. The relation between the two sets of coordinates is obtained by summation of products of appropriate interpolatory polynomials

$$P = \sum_{m=1}^{N} P_m R^n_{i_m}(\xi_1) R^n_{j_m}(\xi_2) R^n_{k_m}(\xi_3) R^n_{l_m}(\xi_4) \tag{3}$$

being $R^n_i$, the $i$th member of the family of Silvester polynomials of degree $n$[1].

For $n = 2$, the transformation is quadratic, thus, a solid delimited by four paraboloid sections is generated; an example is given in Fig. 1(b). Higher order transformations can be used to improve the accuracy in geometric modeling, nevertheless, in practice, it is often desirable to represent geometries that cannot be represented in polynomial form as, for instance, spheres, circular cylinders, and quadric surfaces, in general.

In order to extend the set of representable boundaries, [9] proposed the use of rational Bézier tetrahedra, which provide considerably more flexibility than the Lagrange family. Actually, the polynomial transformation is included as a special case. The mathematical expression for the position vector in a rational Bézier tetrahedron of degree $n$ is

$$P = \frac{\sum_{m=1}^{N} P_m \beta_m B^n_{\boldsymbol{i}_m}(\boldsymbol{\xi})}{\sum_{m=1}^{N} \beta_m B^n_{\boldsymbol{i}_m}(\boldsymbol{\xi})} \tag{4}$$

where $\boldsymbol{i}_m$ stands for the four-tuple $(i_m, j_m, k_m, l_m)$, defined exactly as for the case of Lagrange elements, and $B^n_{\boldsymbol{i}}(\boldsymbol{\xi})$ is the generalized Bernstein polynomial of degree $n$[8]

$$B^n_{\boldsymbol{i}}(\boldsymbol{\xi}) = \frac{n!}{i!j!k!l!} \xi_1^i \xi_2^j \xi_3^k \xi_4^l. \tag{5}$$

$P_m$ are control points, called Bézier points, and the real numbers $\beta_m$ are the associated weights. The number of control points needed is equal to the number of interpolation points required for a polynomial mapping of the same order, but control points, except those associated with vertices, are not necessarily interpolated. For each face, the points at vertices and their two neighbors on edges determine the tangent planes at the corners. An example for $n = 2$ is shown in Fig. 2(b).

If all the weights are equal, (4) becomes a polynomial transformation; the weights can be used as additional degrees of freedom, thus providing a significant increase in versatility. In particular, by properly choosing control points and weights, volumes delimited by quadric surfaces can be exactly represented through a quadratic $(n = 2)$ rational Bézier transformation [8].

The procedure presented in this paper combines rational Bézier tetrahedra with the higher order interpolatory vector bases of curl conforming type proposed in [15]. Bases of arbitrary order can be generated in a systematic way on curvilinear elements by considering the correct expression of the coordinate mapping and of its derivatives.

## III. Finite-Element Hybrid Formulation

The system under consideration is a generic multiport junction whose walls are assumed perfect electric or magnetic conductors.

The FEM is applied in the inner region of the junction $V$ that may be arbitrarily shaped and is allowed to contain inhomogeneous, anisotropic, and lossy materials. In such a region, assumed source free, a time–harmonic electric field must satisfy the vector wave equation

$$\nabla \times \overline{\overline{\mu}}_r^{-1} \nabla \times \mathbf{E} + \overline{\overline{\epsilon}}_r k_0^2 \mathbf{E} = 0 \tag{6}$$

where $\bar{\bar{\epsilon}}_r$ and $\bar{\bar{\mu}}_r$ are the complex relative permittivity and permeability tensors, respectively, and $k_0$ is the free-space wavenumber. A time dependence $e^{j\omega t}$ is assumed and suppressed.

The FEM numerical solution of (6) has been presented before [12], [16]. The region under analysis is subdivided into tetrahedra, and the field is expanded in terms of the given bases [15]. Equation (6) is then cast into a matrix equation via a Galerkin weighted residual approach. Such a formulation implies a surface integral over the device boundary, which is nonzero only at the device ports, which are assumed planar, and where a modal expansion for the tangential components of the field can be enforced in the form

$$\mathbf{H}_{t_k} = \sum_{p_k=1}^{M_k} (b_{p_k} - a_{p_k})\, \mathbf{h}_{p_k} \tag{7}$$

with being $M_k$ the number of modes considered at port $k$, $\mathbf{h}_{p_k}$ being the $p$th tangential magnetic-field eigenfunction, and $a_{p_k}$ and $b_{p_k}$ being the relevant incident and reflected wave amplitudes, respectively. These latter will be cast into two single global vectors $\{a\}$ and $\{b\}$ by resorting to a global numbering scheme $j$.

The matrix equation is then [16]

$$([S] - k_0^2[T])\{E\} = [P]\{a\} - [P]\{b\} \tag{8}$$

where $\{E\}$ is the vector of the coefficients of the unknown field expansion, while $[S]$ and $[T]$ contain the volume integral contributions and $[P]$ contain the surface integrals at the ports.

These matrices are assembled on an element-by-element basis and, for each given element $e$, they are defined by

$$S_{ij}^e = \int\int\int_{V^e} \nabla \times \mathbf{w}_i^e(\mathbf{r}) \cdot \bar{\bar{\mu}}_r^{-1} \nabla \times \mathbf{w}_j^e(\mathbf{r}) dV \tag{9}$$

$$T_{ij}^e = \int\int\int_{V^e} \mathbf{w}_i^e(\mathbf{r}) \cdot \bar{\bar{\epsilon}}_r \mathbf{w}_j^e(\mathbf{r}) dV \tag{10}$$

$$P_{ij}^e = jk\zeta \int\int_{S_p} \mathbf{w}_i^e \cdot \mathbf{h}_j \times \hat{\mathbf{n}} dS. \tag{11}$$

Since both $\{E\}$ and $\{b\}$ are unknown, additional equations are needed to solve (8), hence, the continuity of the tangential electric field at the ports is explicitly imposed, again by applying a modal expansion [16]

$$\mathbf{E}_{t_k} = \sum_{p_k=1}^{M_k} (a_{p_k} + b_{p_k})\, \mathbf{e}_{p_k} \tag{12}$$

and, hence,

$$[C]\{E\} = [D]\{a\} + [D]\{b\} \tag{13}$$

where, again, $[C]$ is computed element by element as

$$C_{ij}^e = \int\int_{S_p} \mathbf{e}_i \cdot \mathbf{w}_j^e dS \tag{14}$$

while $[D]$ is defined on the entire port

$$D_{ij} = \int\int_{S_p} \mathbf{e}_i \cdot \mathbf{e}_j dS. \tag{15}$$

The global system to be solved then comprises (8) and (13), providing both the electric-field distribution within the junction and the scattering coefficients at ports.

The bases and the integration limits of (9)–(11) and (14) are more simply expressed in local coordinates, therefore, it is more convenient to carry out the integrations in the local space. To transform the variables and the region with respect to which the integration is made, a standard process is used, leading to [for the volumetric integral case (9) and (10)]

$$\int\int\int_V f(\mathbf{r}) dV = \int_0^1 \int_0^{1-\xi_1} \int_0^{1-\xi_1-\xi_2} f(\boldsymbol{\xi})\, |\bar{\bar{J}}|\, d\xi_1 d\xi_2 d\xi_3 \tag{16}$$

where $|\bar{\bar{J}}|$ denotes the Jacobian of the coordinate transformation, which can be expressed as

$$|\bar{\bar{J}}| = \boldsymbol{\ell}^1 \cdot \boldsymbol{\ell}^2 \times \boldsymbol{\ell}^3 \tag{17}$$

being $\boldsymbol{\ell}^q$, the so-called *unitary basis vectors* [15]

$$\boldsymbol{\ell}^q = \frac{\partial \mathbf{r}}{\partial \xi_q}, \qquad q = 1, 2, 3. \tag{18}$$

In order to perform the integrations in the local space, it is necessary to express the global derivatives occurring in (9) in terms of local derivatives. This is easily done by exploiting the relation

$$\nabla \xi_i = \frac{\boldsymbol{\ell}^j \times \boldsymbol{\ell}^k}{|\bar{\bar{J}}|} \tag{19}$$

where $i, j, k$ are taken in cyclic order.

The key step for the integral computation is, therefore, the determination of unitary basis vectors. By recalling the dependence of the fourth local variable, for the polynomial mapping presented in Section II, the following expression is obtained:

$$\boldsymbol{\ell}^q = \sum_{M=1}^{N} P_m \left[ \prod_{\substack{r=1 \\ r \neq q}}^{4} R^n_{I(r,m)}(\xi_r) \frac{dR^n_{I(q,m)}(\xi_q)}{d\xi_q} + \right. \\ \left. - \prod_{r=1}^{3} R^n_{I(r,m)}(\xi_r) \frac{dR^n_{I(4,m)}(\xi_4)}{d\xi_4} \right] \tag{20}$$

where $I(r,m)$ is the $r$th index of the four-tuple $\boldsymbol{i}_m$.

Similarly, for rational Bézier elements, it is

$$\boldsymbol{\ell}^q = \left\{ \left[ \sum_{m=1}^{N} P_m \beta_m \frac{\partial B^n_{\boldsymbol{i}_m}(\boldsymbol{\xi})}{\partial \xi_q} \right] \cdot \left[ \sum_{m=1}^{N} \beta_m B^n_{\boldsymbol{i}_m}(\boldsymbol{\xi}) \right] \right. \\ \left. - \left[ \sum_{m=1}^{N} P_m \beta_m B^n_{\boldsymbol{i}_m}(\boldsymbol{\xi}) \right] \cdot \left[ \sum_{m=1}^{N} \beta_m \frac{\partial B^n_{\boldsymbol{i}_m}(\boldsymbol{\xi})}{\partial \xi_q} \right] \right\} \cdot \\ \cdot \left[ \sum_{m=1}^{N} \beta_m B^n_{\boldsymbol{i}_m}(\boldsymbol{\xi}) \right]^{-2}. \tag{21}$$

It is worth pointing out that the computational complexity is almost the same for coordinates mappings (3) and (4), as confirmed by computation time required for simulations. Indeed, only polynomials of degree at most $n$ are involved in calculations. Besides, partial derivatives appearing in (21) can be easily

written in terms of lower order Bernstein polynomials by exploiting the following relation:

$$\frac{\partial B^n_{\boldsymbol{i}}(\boldsymbol{\xi})}{\partial \xi_q} = \frac{n}{n-1}\left[B^{n-1}_{(i-\delta^1_q, j-\delta^2_q, k-\delta^3_q, l)}(\boldsymbol{\xi}) - B^{n-1}_{(i,j,k,l-1)}(\boldsymbol{\xi})\right] \tag{22}$$

where $B^n_{(i,j,k,l)}$ is assumed to be zero if one of the indexes $(i, j, k, l)$ is zero or less.

The integrals in (11) and (14) are performed in a similar way. The relevant triangular faces may have curved sides and curved triangular elements can be obtained from (3) or (4) by simply setting one barycentric coordinate equal to zero. Surface integrals are then computed over the other three local coordinates involved.

The integrations are carried out numerically, by using 512- and 64-point Gaussian quadrature formula on tetrahedral and triangular domains, respectively [17].

It is worth noting that, if only scattering parameters are needed, an efficient solution algorithm can be applied: the unknown $\{E\}$ can be eliminated within the solving system yielding to a linear system with a full coefficient matrix, but with much smaller dimensions than the original one [10, pp. 104–105].

## IV. Numerical Results

The procedure has been tested on some examples for which measured results were available. Examples were chosen with increasing relevance of the device curved features to show how the Bézier mapping allows a comparably lower number of elements. The number of elements is indeed decreasing from one example to the next. The mesh chosen is the one with the least possible elements, yet exactly matching, with the Bézier mapping, the device structure. The order of the bases is the lowest yielding good results for the given mesh. Reference [9] presents an investigation on the performances of different orders of bases over a given mesh.

As a first example, two crossed metal posts in a WR-62 waveguide ($a = 15.7988$ mm, $b = 7.8994$ mm) have been considered. Second-order basis functions on a rather dense mesh of 273 tetrahedra, corresponding to 5709 FEM unknowns, and four modes on each port have been considered. In Fig. 3, the reflection coefficient of the fundamental mode at one port is shown; results provided by simulations with rectilinear (linear mapping) and curved (rational Bézier mapping) elements are compared with measures presented in [18]. It can be seen that the use of the proposed curved elements allows to achieve a greater accuracy, especially in the peak region. Conventional polynomial mapping is not shown, here, for the sake of clarity, since its results are comparable with the ones yielded by the Bézier mapping. This similarity is due to the fact that the radius of curvature of the posts is very small in terms of wavelength. Polynomial mapping is, hence, shown in subsequent figures, where differences are relevant.

Next, a Y-junction circulator in rectangular waveguide ($a = 22.86$ mm, $b = 11.43$ mm) with a TT1–109 circular ferrite post has been analyzed. Material parameters are given in [19]; magnetic and dielectric losses have been taken into account and a

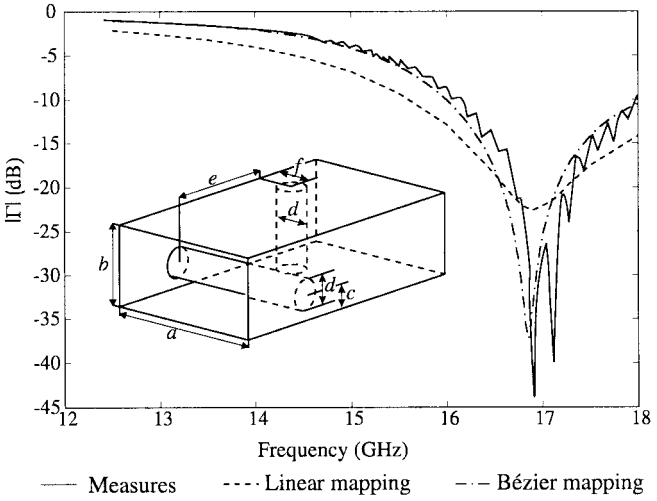


Fig. 3. Magnitude of reflection coefficient for two crossed posts in WR-62 waveguide. Dimensions: $a = 15.7988$ mm, $b = 7.8994$ mm, $c = 2.5$ mm, $d = 3$ mm, $e = 11.51$ mm, $f = 4$ mm. Measured values are compared with the results provided by simulations with different types of mapping.

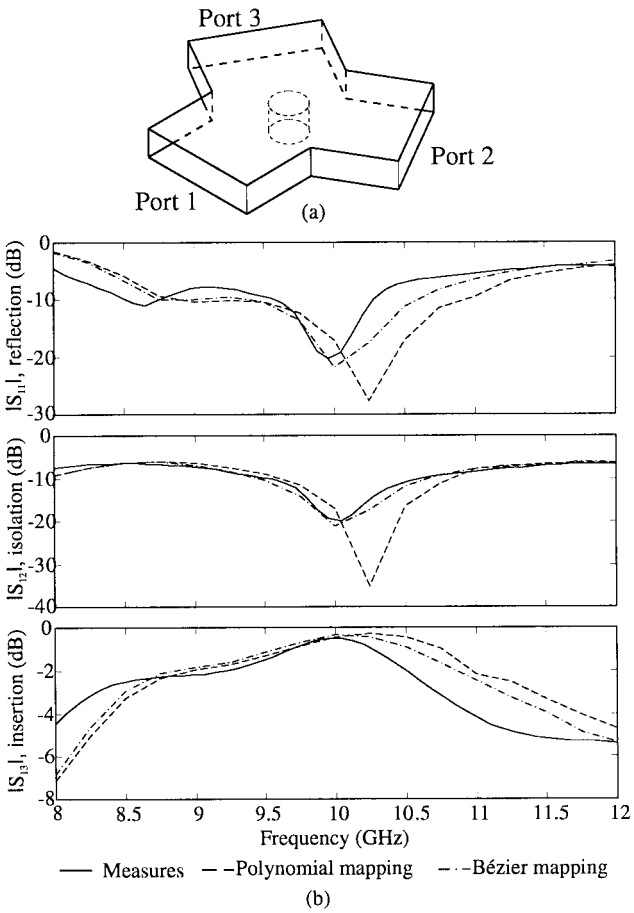


Fig. 4. Magnitude of the insertion, isolation, and reflection parameters for an $H$-plane Y-junction with a TT1–109 circular ferrite post having a diameter of 7 mm. (a) Geometry of the junction. (b) Comparison between measured values and results provided by simulations with different types of mapping.

200-Oe internal dc magnetic field has been assumed. The calculations have been carried out by using ten waveguide modes on each port, 95 curved elements, and first-order basis functions (826 FEM unknowns). The performances of the junction for the fundamental $\mathrm{TE}_{10}$ mode are shown in Fig. 4, where the

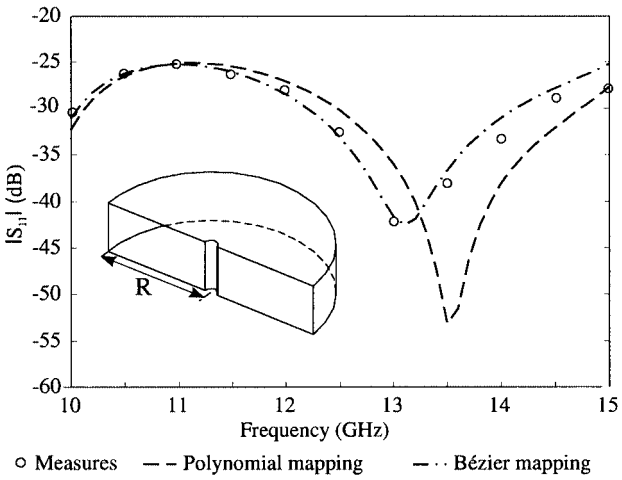


Fig. 5. Analysis of a 180° $H$-plane bend with $R = 20.225$ mm. Magnitude of reflection coefficient versus frequency: comparison between measured values [20] and simulations performed using different types of mapping.

results obtained by applying the polynomial interpolatory (3) and proposed (4) mappings are compared with experimental results [19]. It is evident that, with the polynomial mapping, the agreement with measures is not as good as with the rational one, especially as far as the value of the circulation frequency is concerned.

As a further example, simulations have been performed on a 180° $H$-plane bend in an WR-75 waveguide ($a = 19.05$ mm, $b = 9.525$ mm). In order to demonstrate the greater robustness to mesh distortion of the proposed mapping, the structure has been discretized with a rather coarse asymmetric mesh composed of 58 elements. Third-order basis functions, corresponding to 2056 FEM unknowns, have been used. Simulation results, shown in Fig. 5, demonstrate the greater accuracy provided by the proposed mapping.

## V. Conclusions

The enhancement of a hybrid procedure combining FEM and modal expansions for the analysis of generic 3-D microwave multiport junctions has been presented based on a rational Bézier mapping for the definition of curved elements, together with higher order bases. Numerical results have demonstrated that the proposed elements can yield a much greater accuracy compared to rectilinear and conventional curved ones.

## References

[1] P. P. Silvester and R. L. Ferrari, *Finite Elements for Electrical Engineers*, 3rd ed. Cambridge, U.K.: Cambridge Univ. Press, 1996.
[2] O. C. Zienkiewicz, *The Finite Element Method*, 3rd ed. New York: McGraw-Hill, 1977.
[3] C. W. Crowley, P. P. Silvester, and H. Hurwitz, Jr., "Covariant projection elements for 3-D vector field problems," *IEEE Trans. Magn.*, vol. MAG-24, pp. 397–400, Jan. 1988.
[4] J. P. Webb and R. Miniowitz, "Analysis of 3-D microwave resonators using covariant-projection elements," *IEEE Trans. Microwave Theory Tech.*, vol. 29, pp. 1895–1899, Nov. 1991.
[5] J. S. Wang and N. Ida, "Curvilinear and higher order 'edge' finite elements in electromagnetic field computation," *IEEE Trans. Magn.*, vol. 29, pp. 1491–1494, Mar. 1993.
[6] S. L. Foo and P. P. Silvester, "Finite element analysis of inductive strips in unilateral finlines," *IEEE Trans. Microwave Theory Tech.*, vol. 41, pp. 298–304, Feb. 1993.
[7] S. Selleri, "A new class of NURBS based hybrid hyperparametric elements," in *Actes J. Int. Nice sur les Antennes*, Nice, France, Nov. 1998, pp. 165–168.
[8] J. Hoschek and D. Lasser, *Fundamentals of Computer Aided Geometric Design*. Wellesley, MA: A. K. Peters, 1993.
[9] E. Martini and S. Selleri, "Innovative class of curvilinear tetrahedral elements," *Electron. Lett.*, vol. 37, no. 9, pp. 557–558, Sept. 2001.
[10] G. Pelosi, R. Coccioli, and S. Selleri, *Quick Finite Elements for Electromagnetic Waves*. Boston, MA: Artech House, 1998.
[11] K. Ise, K. Inoue, and M. Koshiba, "Three-dimensional finite-element solution of dielectric scattering obstacles in a rectangular waveguide," *IEEE Trans. Microwave Theory Tech.*, vol. 38, pp. 1352–1359, Sept. 1990.
[12] J. Rubio, J. Arroyo, and J. Zapata, "Analysis of passive microwave circuits by using a hybrid 2-D and 3-D finite-element mode-matching method," *IEEE Trans. Microwave Theory Tech.*, vol. 47, pp. 1746–1749, Sept. 1999.
[13] H. B. Lee and T. Itoh, "A systematic optimum design of waveguide-to-microstrip transition," *IEEE Trans. Microwave Theory Tech.*, vol. 45, pp. 803–809, May 1997.
[14] K. Hirayama, M. S. Alam, Y. Hayashi, and M. Koshiba, "Vector finite element method with mixed- interpolation-type triangular-prism element for waveguide discontinuities," *IEEE Trans. Microwave Theory Tech.*, vol. 42, pp. 2311–2316, Dec. 1994.
[15] R. D. Graglia, D. R. Wilton, and A. F. Peterson, "Higher order interpolatory vector bases for computational electromagnetics," *IEEE Trans. Antennas Propagat.*, vol. 45, pp. 329–342, Mar. 1997.
[16] E. Limiti, E. Martini, G. Pelosi, M. Pierozzi, and S. Selleri, "Efficient hybrid finite elements-modal expansion method for microstrip-to-waveguide transition analysis," *J. Electromagn. Waves Applicat.*, vol. 15, pp. 1027–1035, 2001.
[17] A. H. Stroud, *Approximate Calculation of Multiple Integrals*. Englewood Cliffs, NJ: Prentice-Hall, 1971.
[18] R. Bunger and F. Arndt, "Moment-method analysis of arbitrary 3-D metallic n-port waveguide structures," *IEEE Trans. Microwave Theory Tech.*, vol. 48, pp. 531–537, Apr. 2000.
[19] J. B. Castillo, Jr. and L. E. Davis, "Computer-aided design of three-port waveguide junction circulators," *IEEE Trans. Microwave Theory Tech.*, vol. MTT-18, pp. 25–34, Jan. 1970.
[20] P. Cornet, R. Dusséaux, and J. Chandezon, "Wave propagation in curved waveguides of rectangular cross section," *IEEE Trans. Microwave Theory Tech.*, vol. 47, pp. 965–972, July 1999.

**Enrica Martini** (S'98–M'02) was born in Spilimbergo, Italy. She received the Laurea degree (*cum laude*) in telecommunications engineering and Ph.D. degree in informatics and telecommunications from the University of Florence, Florence, Italy, in 1998 and 2002, respectively, and the Ph.D. degree in electronics from the University of Nice-Sophia Antipolis, Nice-Sophia Antipolis, France, in 2002.

From 1998 to 1999, she was with the University of Florence, during which time she worked under a one-year research grant from the Alenia Aerospazio Company, Rome, Italy. She is currently a Research Associate with the University of Siena, Siena, Italy. Her research interests include high-frequency techniques for scattering problems and the application of the FEM to the analysis of microwave passive components.

**Giuseppe Pelosi** (M'88–SM'91–F'00) was born in Pisa, Italy. He received the Laurea (Doctor) degree (*summa cum laude*) in physics from the University of Florence, Florence, Italy, in 1976.

Since 1979, he was with the Department of Electronics and Telecommunications, University of Florence, where he is currently a Full Professor. In 1994 and 1995, he was a Visiting Scientist with McGill University, Montreal, QC, Canada. He has been mainly involved in research in the field of numerical and asymptotic techniques for applied electromagnetics. He coauthored *Finite Elements for Wave Electromagnetics* (Piscataway, NJ: IEEE Press, 1994), *Finite Element Software for Microwave Engineering* (New York: Wiley, 1996), and *Quick Finite Elements for Electromagnetic Fields* (Norwood, MA: Artech House, 1998). His past research were extensions and applications of the geometrical theory of diffraction, as well as methods for radar cross-sectional analysis of complex targets. His current research activity is mainly devoted to the development of numerical procedures in the context of the FEM, with particular emphasis on microwave and millimeter-wave engineering (antennas, circuits, devices, and scattering problems).

Dr. Pelosi is a member of the Board of the Directors of the Applied Computational Electromagnetics Society.

**Stefano Selleri** (S'92–M'96–SM'03) was born in Viareggio, Italy, on December 9, 1968. He received the Laurea degree (*cum laude*) in electronic engineering and Ph.D. degree in computer science and telecommunications from the University of Florence, Florence, Italy, in 1992 and 1997, respectively.

In 1992, he was a Visiting Scholar with The University of Michigan at Ann Arbor. In 1994, he was a Visiting Scholar with McGill University, Montreal, QC, Canada. In 1997, he was a Visiting Scholar with the Laboratoire d'Electronique, University of Nice-Sophia Antipolis, Nice-Sophia Antipolis, France. From February to July 1998, he was a Researcher with the Centre National d'Etudes Telecommunications (CNET), France Telecom, La Turbie, France. He is currently an Assistant Professor with the University of Florence, where he conducts research on numerical modeling of microwave devices and circuits.